Three-wave gap solitons in waveguides with quadratic nonlinearity

William C. K. Mak,[1,*] Boris A. Malomed,[2,†] and P. L. Chu[1,‡]
[1]*Optical Communications Group, School of Electrical Engineering, University of New South Wales, Kensington, New South Wales 2052, Australia*
[2]*Department of Interdisciplinary Studies, Faculty of Engineering, Tel Aviv University, Tel Aviv 69978, Israel*
(Received 3 April 1998; revised manuscript received 6 July 1998)

A model of the second-harmonic-generating ($\chi^{(2)}$) optical medium with a Bragg grating is considered. Two components of the fundamental harmonic (FH) are assumed to be resonantly coupled through the Bragg reflection, while the second harmonic (SH) propagates parallel to the grating, hence its dispersion (diffraction) must be explicitly taken into consideration. It is demonstrated that the system can easily generate stable three-wave gap solitons of two different types (*free-tail* and *tail-locked* ones) that are identified analytically according to the structure of their tails. The stationary fundamental solitons are sought for analytically, by means of the variational approximation, and numerically. The results produced by the two approaches are in fairly reasonable agreement. The existence boundaries of the soliton are found in an exact form. The stability of the solitons is determined by direct partial differential equation simulations. A threshold value of an effective FH-SH mismatch parameter is found, the soliton being stable above the threshold and unstable below it. The stability threshold strongly depends on the soliton's wave-number shift k and very weakly on the SH diffraction coefficient. Stationary two-soliton bound states are found, too, and it is demonstrated numerically that they are stable if the mismatch exceeds another threshold, which is close to that for the fundamental soliton. At $k<0$, the stability thresholds do not exist, as *all* the fundamental and two-solitons are stable. With the increase of the mismatch, the two-solitons disappear, developing a singularity at another, very high, threshold. The existence of the stable two-solitons is a drastic difference of the present model from the earlier investigated $\chi^{(2)}$ systems. It is argued that both the fundamental solitons and two-solitons can be experimentally observed in currently available optical materials with the quadratic nonlinearity.
[S1063-651X(98)09811-0]

PACS number(s): 42.65.Tg

I. INTRODUCTION

The idea of using the large nonlinear phase shift generated by cascaded quadratic effects in the second-harmonic-generation (SHG) systems to balance dispersion or diffraction so as to produce localized solitary waves (or simply solitons, in a mathematically nonrigorous sense) was proposed long ago [1] A soliton due to a nonlinear parametric interaction of a more general type, viz., the three-wave resonant interaction (3WRI), is also possible in the presence of the quadratic nonlinearity. It differs from the simplest two-wave interaction in that there are two physically different fundamental-harmonic (FH) components, corresponding to different polarizations. The two orthogonally polarized FH waves generate a single second-harmonic (SH) field through the so-called type-II phase matching [2], the SH field being down-converted to both components of the FH field. In situations where the dispersion and diffraction can be neglected, a number of investigations have been carried out on this topic [3]. Note that the 3WRI model with group-velocity differences between the waves but *without* diffraction or dispersion is exactly integrable by means of the inverse scattering transform [4] (moreover, this model is integrable, too, in the multidimensional case).

Theoretical studies of the 3WRI in the presence of the diffraction or dispersion have commenced recently [5–7]. In [6] particular exact soliton solutions were found; in [7] a general two-parameter family of solitons was constructed by means of both the variational approximation (VA) and direct numerical methods and domains of stable and unstable solitons were identified. Further results concerning the stability of the solitons supported by the 3WRI can be found in [8,9]. In [9] it was pointed out that the 3WRI may give rise to a multistability of the soliton solutions in a limited range of parameters.

In the present work the aim is to study three-wave *gap solitons* in $\chi^{(2)}$ media equipped with a resonant grating, which gives rise to a strong effective dispersion or diffraction (the grating is resonant if its spacing is commensurable with the wavelength, leading to the resonant Bragg reflection of light). This advantage offered by the grating is very important because, having a strong dispersion/diffraction, it is much easier to achieve the FH-SH phase matching, which is the fundamental condition necessary for the use of the $\chi^{(2)}$ nonlinearity. Theoretical results for the four-wave gap solitons in the temporal domain, supported by SHG in combination with the Bragg gratings, can be found in [10]. In the present work we consider a waveguiding structure that carries the grating in the form of a system of parallel scores along the propagation direction Z, which will give rise to *three-wave* spatial solitons: The grating will couple two FH waves $E_{1,2}$ to each other through the resonant Bragg scattering and to the SH wave E_3 through the nonlinearity. The two

*Electronic address: w.mak@alpha400.ee.unsw.edu.au
†Electronic address: malomed@eng.tau.ac.il
‡Electronic address: p.chu@unsw.edu.au

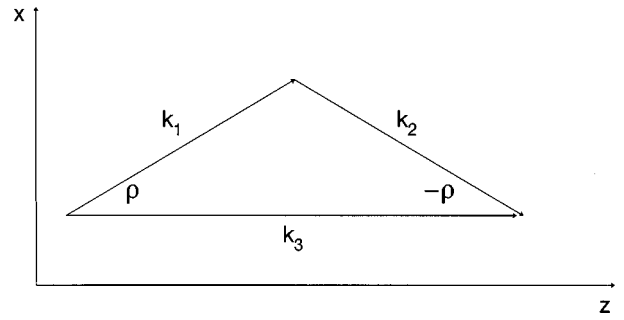

FIG. 1. Configuration of the wave vectors $\mathbf{k}_1$, $\mathbf{k}_2$, and $\mathbf{k}_3$ of the two components of the fundamental harmonic and of the second harmonic. The scores that form the spatial grating are parallel to the z axis.

FH waves are chosen so that their carrier wave vectors have equal lengths, making opposite angles with the Z axis (i.e., with the scores that form the grating), while the SH wave vector is parallel to Z (Fig. 1). The mathematical model of this system includes transverse-walkoff terms in the equations for the two FH components, whose effect is definitely much stronger than that of the intrinsic diffraction. That is why the diffraction terms may be dropped in the FH equations [7]. However, the diffraction must be kept in the SH equation (along with the phase-mismatch term), as this harmonic does not interact with the grating parallel to its wave vector.

A similar model was a starting point in the work [11], but a crucial difference is that a very large phase mismatch between the SH and FHs was assumed to allow one to eliminate the SH component, transforming the system into the *massive Thirring model* (MTM) [12], which is exactly integrable by means of the inverse scattering transform [13] [an optical fiber with the Bragg grating and *cubic* (Kerr) nonlinearity is described by a well-known nonintegrable generalization of the MTM [14]]. Since all the soliton solutions of the integrable MTM are stable, the solitons considered in [11] are also always stable. In the present work we do not assume that the phase mismatch is especially large and keep the SH component in the model explicitly. Obviously, the case of a smaller mismatch is more physically interesting. We will demonstrate that stable three-wave soliton solutions do exist at a large mismatch and they continue to exist as the phase mismatch is decreased. However, we find a *threshold value* of the mismatch, below which the soliton solutions lose their stability (though they do not disappear). An instability threshold in terms of the mismatch parameter is also known for the usual $\chi^{(2)}$ solitons [7,8,15]; however, the principal difference is that the usual solitons are *stable* in the fully matched case, while our solitons may be both stable and unstable in this case, depending on other parameters (the wave-number shift and an effective SH diffraction parameter), i.e., the location of the instability threshold is different in the present model. We also investigated the effect of changing the SH diffraction (dispersion) coefficient, finding that it has less effect on the threshold than the wave number shift and the wave-vector mismatch.

Finally, we will consider two-soliton bound-state solutions (or simply two-solitons), finding that they have their own stability threshold (which is higher than but close to the one for the fundamental solitons). The fact that two-solitons in our model can be stable is quite nontrivial as, in the usual $\chi^{(2)}$ models, all the higher-order solitons are subject to an instability [16,17].

The rest of the paper is organized as follows. In Sec. II a detailed formulation of the model is given. In Sec. III we consider the linearized version of the model, with the aim to investigate a possible structure of the soliton's tails. Though the analysis of the linearized system is very simple, it yields fairly useful information about a parametric region in which the solitons may exist and allows us to identify two different possible types of the solitons, which we call *free-tail* and *tail-locked* solitons. Actually, the tails of the solitons of the latter type cannot be described by the fully linearized system; instead, the relevant system is *semilinear*, in which only the FH equation is linearized. In Sec. IV we briefly describe analytical and numerical techniques to be used for the study of both the stationary shape of the solitons and their stability in the full nonlinear system. The analytical approach is based on the VA, its peculiarity being that one should devise a tractable ansatz for the complex FH soliton's component. In Sec. V the results concerning the existence and stability of the fundamental solitons are displayed and in Sec. VI similar results are displayed for the two-solitons. The results obtained in the work are summarized in Sec. VII.

II. MODEL

We consider the resonant nonlinear interaction of two FH waves with identical frequencies ω and Z components of their carrier wave vectors k_1 and k_2. The $\chi^{(2)}$ nonlinearity generates the third wave with wave number k_3 at the frequency 2ω. The case of interest is $\Delta k \ll k_3$, where $\Delta k \equiv k_1 + k_2 - k_3$ is the wave-vector mismatch. We assume that the FH wave vectors make small angles $\pm\rho$ with the Z direction and have the same length, so that $k_1 = k_2 \equiv k$; see Fig. 1. Assuming the amplitudes E_1, E_2, and E_3 of the interacting harmonics to be slowly varying in comparison to the carrier waves and employing known asymptotic techniques [18], one can derive the following system of the amplitude equations:

$$2ik\frac{\partial E_1}{\partial Z} + 2ik\rho\frac{\partial E_1}{\partial X} + \lambda E_2 + \chi E_3 E_2^* e^{-i\Delta kZ} = 0,$$

$$2ik\frac{\partial E_2}{\partial Z} - 2ik\rho\frac{\partial E_2}{\partial X} + \lambda E_1 + \chi E_3 E_1^* e^{-i\Delta kZ} = 0, \qquad (1)$$

$$2ik_3\frac{\partial E_3}{\partial Z} + \frac{\partial^2 E_3}{\partial X^2} + \tilde{\chi} E_1 E_2 e^{i\Delta kZ} = 0,$$

where $\chi \equiv (4\pi\omega^2/kc^2)\chi^{(2)}(\omega; 2\omega, -\omega)$ and $\tilde{\chi} \equiv (8\pi\omega^2/k_3c^2)\chi^{(2)}(2\omega; \omega, \omega)$, λ being the coupling constant induced by the Bragg scattering. We can then rescale Eq. (1) by setting $E_1 \equiv \lambda v_1/\sqrt{\chi\tilde{\chi}}$, $E_2 \equiv \lambda v_2/\sqrt{\chi\tilde{\chi}}$, $E_3 \equiv (\lambda/\chi)v_3 \exp(i\Delta kZ)$, $Z \equiv 2kz/\lambda$, and $X \equiv 2\rho kx/\lambda$. Additionally, using the fact that $k_3/k \approx 2$ and defining the effective mismatch $q \equiv 4k\Delta k/\lambda$ and the diffraction parameter $D \equiv \lambda/4\rho^2k^2$, we arrive at the system in the normalized form

$$i\frac{\partial v_1}{\partial z}+i\frac{\partial v_1}{\partial x}+v_2+v_3v_2^*=0,$$

$$i\frac{\partial v_2}{\partial z}-i\frac{\partial v_2}{\partial x}+v_1+v_3v_1^*=0, \tag{2}$$

$$2i\frac{\partial v_3}{\partial z}-qv_3+D\frac{\partial^2 v_3}{\partial x^2}+v_1v_2=0.$$

Using obvious symmetry properties of the system (2), we can confine ourselves to the case $D>0$ without the loss of generality.

We are interested in stationary solutions to Eqs. (2), in the form $v_1=e^{ikz}u_1(x)$, $v_2=e^{ikz}u_2(x)$, and $v_3=e^{2ikz}u_3(x)$, where k is a common wave-number shift of the harmonics. Thus we obtain from Eqs. (2) a system

$$-ku_1+iu_1'+u_2+u_3u_2^*=0,$$

$$-ku_2-iu_2'+u_1+u_3u_1^*=0, \tag{3}$$

$$-(4k+q)u_3+Du_3''+u_1u_2=0,$$

the prime standing for d/dx. We can impose a natural reduction $u_1=-u_2^*\equiv u$ on the amplitudes u_1 and u_2, which is compatible with Eqs. (2). Substituting this into Eqs. (3), we finally obtain the equations for the complex function $u(x)$ and real $u_3(x)$,

$$-ku+iu'-u_3u-u^*=0, \tag{4a}$$

$$-(4k+q)u_3+Du_3''-|u|^2=0. \tag{4b}$$

This is the simplest version of the model to produce the three-wave solitons in the $\chi^{(2)}$ media.

III. LINEARIZED AND SEMILINEARIZED SYSTEMS

First of all, it is useful to analyze the linearized version of the system (4). Obviously, the linearized equations get decoupled. Looking for a solution to them in the form

$$u\sim\exp(-\mu|x|),\quad u_3\sim\exp(-\mu_3|x|), \tag{5}$$

corresponding to an exponentially decaying tail of the soliton, it is straightforward to find

$$\mu^2=1-k^2,\quad \mu_3^2=D^{-1}(4k+q). \tag{6}$$

A necessary condition for the existence of the soliton is $\mu^2>0$, i.e., according to Eq. (6), $|k|<1$. This restriction on the allowed values of the propagation constant implies that we are dealing with *gap solitons*, which is typical for all the model involving the Bragg scattering [14]. Another necessary condition $4k+q>0$ is imposed by demanding $\mu_3^2>0$ (recall that we set, by definition, $D>0$). However, the expression (6) for μ_3^2 makes sense only if $\mu_3\leqslant 2\mu$ or, in an explicit form,

$$q\leqslant q_0(k)\equiv 4D(1-k^2)-4k; \tag{7}$$

otherwise the quadratic term in Eq. (4b) is dominating over the linear ones at $|x|\to\infty$.

Thus we arrive at the conclusion that the χ^2 solitons may be of two different types, within the framework of the same model. In the region (7), supplemented by the necessary condition $|k|<1$, the tails of both the FH and SH components of the soliton are governed by the decoupled linearized equations and have the form given by Eqs. (5) and (6), in which case the solitons can be naturally called *free-tail* ones. However, in the opposite case, the equation for the SH component [Eq. (4b)] *cannot* be linearized, hence the soliton's tails are determined, in this case, by a *semilinear* system

$$-ku+iu'-u^*=0,\quad -(4k+q)u_3+Du_3''=|u|^2. \tag{8}$$

A general solution to Eqs. (8) describing the soliton's tails is obvious [cf. Eqs. (5) and (6)]: If $k<0$,

$$u=A\,\exp\left(\frac{i}{2}\sin^{-1}(\sqrt{1-k^2})\right)\exp(-\sqrt{1-k^2}|x|), \tag{9}$$

$$u_3=A^2[4D(1-k^2)-(4k+q)]^{-1}\exp(-2\sqrt{1-k^2}|x|), \tag{10}$$

A being an arbitrary real constant and, in the case $k>0$, $u\to iu^*$. Of course, the solution (9) for the FH tail is exactly the same as in the case of the free-tail soliton; however, the solution (10) for the SH tail is very different, being locked to the FH tail, so that the solitons of this type may be called *tail locked*. Note that the boundary between the free-tail and tail-locked solitons $q=q_0(k)$ [see Eq. (7)] may also be defined as the point of the *exact matching* between FH and SH, following the analogy with the usual $\chi^{(2)}$ models.

IV. ANALYTICAL AND NUMERICAL TECHNIQUES FOR THE ANALYSIS OF THE NONLINEAR SYSTEM

To find soliton solutions to the full nonlinear equations (4), analytical and numerical methods were employed. An analytical one is based on the VA and then the numerical finite-difference method uses the approximate solutions furnished by the VA as the first guess. Such a two-step approach has proved to be very efficient in a number of other problems, e.g., searching for solitons in the model of tunnel-coupled parallel $\chi^{(2)}$ waveguides [19]. However, there is a different technical feature in the present problem: Thus far the VA was usually applied to find real solutions, while here we are seeking essentially *complex* ones (an exception is the work in [20], in which the VA was elaborated for solitons in the generalized MTM introduced in [14] to describe an optical fiber with the Bragg grating and cubic nonlinearity). This difference is not simply formal: The necessity to accommodate a complex wave form makes a corresponding ansatz (the trial soliton's form) much more involved and in many cases a straightforward extension of the usual VA leads to messy equations of no practical value. However, below we will develop an analytical approximation that will produce very reasonable results for the present model.

To apply the VA we need the Lagrangian for Eqs. (4), $L=\int_{-\infty}^{+\infty}\mathcal{L}\,dx$, with the density

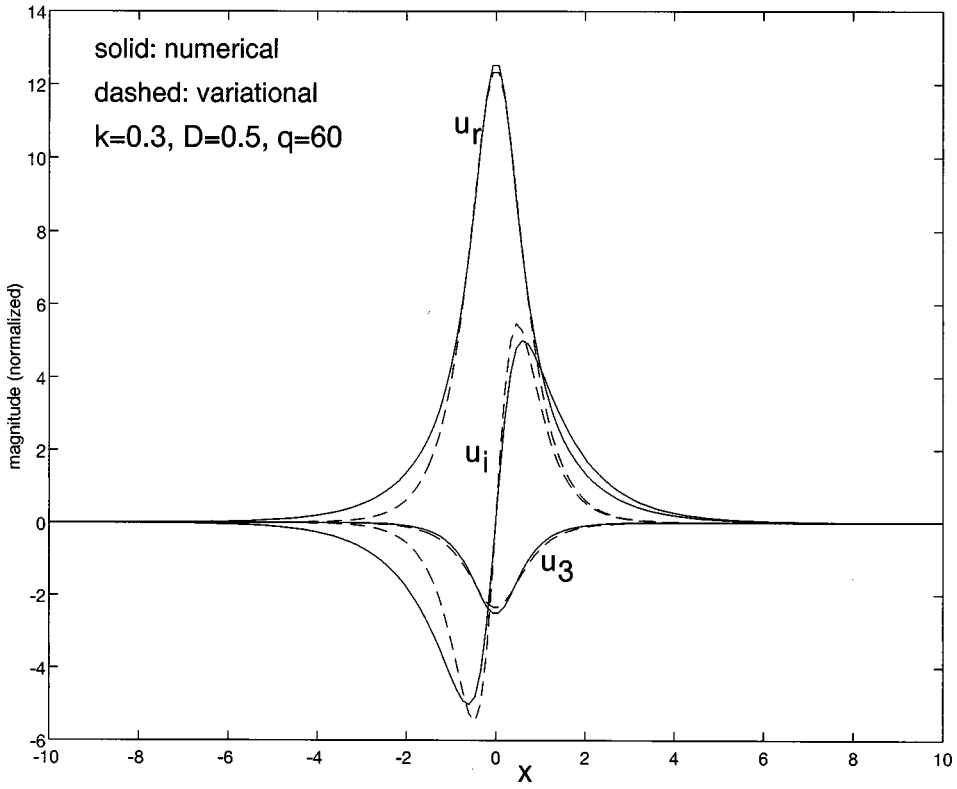

FIG. 2. Typical example of the comparison between the numerical (solid curves) and variational (dashed curves) fundamental-soliton solutions for the real (u_r) and imaginary (u_i) parts of the fundamental-harmonic component and the real second-harmonic component (u_3). The values of the parameters are $k=0.3$, $D=0.5$, and $q=60$.

$$\mathcal{L}=-k|u|^2-\frac{1}{2}(q+4k)u_3^2+\frac{i}{2}[u'u^*-(u^*)'u]$$
$$-\frac{1}{2}D(u_3')^2-|u|^2u_3-\frac{1}{2}[u^2+(u^*)^2]. \tag{11}$$

Then we adopt the following complex ansatz for the solutions sought:

$$u=A\ \mathrm{sech}(\mu x)+iB\ \sinh(\mu x)\mathrm{sech}^2(\mu x),$$
$$u_3=A_3\mathrm{sech}(\mu x), \tag{12}$$

where the soliton's amplitudes A, A_3, and B and the inverse width μ are free parameters to be found by means of the VA. Insertion of Eqs. (12) into Eq. (11) and integration generate an *effective Lagrangian* L. We then follow the variational formalism to derive the VA equations $\partial L/\partial A=0$, $\partial L/\partial B=0$, $\partial L/\partial A_3=0$, and $\partial L/\partial\mu=0$. The resulting algebraic equations are

$$4\mu^{-1}(1+k)A+\frac{4}{3}B+\pi\mu^{-1}AA_3=0,$$
$$\frac{4}{3}\mu^{-1}(1-k)B-\frac{4}{3}A-\frac{\pi}{4}\mu^{-1}A_3B=0,$$
$$2\mu^{-1}(q-4k)A_3-\frac{2}{3}D\mu A_3-\frac{\pi}{8}\mu^{-1}B^2-\frac{\pi}{2}\mu^{-1}A^2=0,$$
$$-\mu^{-2}\left[-2(1+k)A^2+\frac{2}{3}(1-k)B^2+(q-4k)A_3^2\right.$$
$$\left.-\frac{\pi}{2}A^2A_3-\frac{\pi}{8}A_3B^2\right]-\frac{1}{3}DA_3^2=0. \tag{13}$$

This set of algebraic equations was solved numerically. Other details of the procedure are straightforward. After this, the stationary-soliton solutions to Eqs. (4) were obtained by means of a direct finite-difference numerical scheme [21]. The results produced by these methods are displayed and commented upon below.

V. STATIONARY FUNDAMENTAL-SOLITON SOLUTIONS: EXISTENCE AND STABILITY

A comparison of the stationary fundamental-soliton solutions obtained, in a typical case, by means of the analytical and numerical methods is presented in Fig. 2 (a relatively large value of the normalized mismatch, $q=60$, is selected for this figure; however, this corresponds to a point just within the region of stable fundamental solitons; see Fig. 4 below). It is seen that the agreement is acceptable, especially in view of the fairly simple form of the ansatz (12).

In Fig. 3 we present a numerically obtained *family* of the fundamental-soliton solutions to Eqs. (4), in the form of three-dimensional plots showing the dependence of the basic characteristics of the fundamental soliton, viz., the amplitudes of its two components u and u_3 and width of the u component vs the mismatch q and wave-number shift k, the

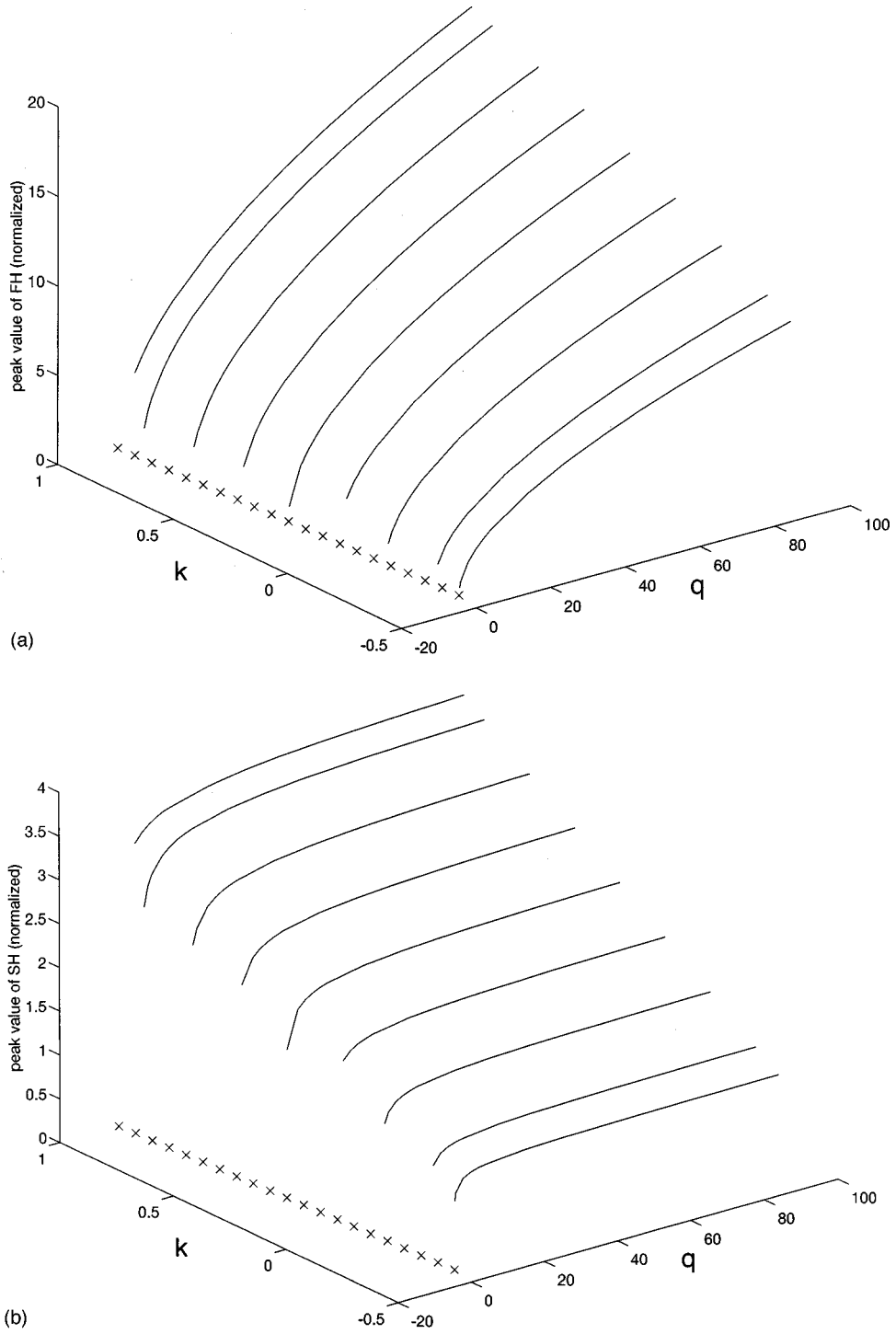

FIG. 3. Family of fundamental-soliton solutions: (a) The FH (u) amplitude, (b) the SH (u_3) amplitude, and (c) the FH width are plotted vs the wave-number shift k and phase mismatch q, while the SH diffraction parameter is fixed at $D=0.5$. The plot for the SH width is similar to (c). The line consisting of crosses shows the existence boundary $4k+q=0$ for the tail-free solitons.

diffraction coefficient D being fixed at a realistic value 0.5. The width of the u_3 component is not displayed, as it turns out to be quite close to (more accurately, slightly smaller than) the u component's width [note that the ansatz (12) adopted above as the basis of the VA assumed both components to have identically equal widths]. Here the standard definition of the full width at half maximum is applied to the absolute values of the complex fields and the amplitudes refer to their peak values. A general trend seen in these plots is that the amplitudes of the soliton's components increase, whereas their widths decrease, with the increase of q and k. Another clearly seen and quite natural feature is that the FH and SH amplitudes are on the same order of magnitude at small values of the mismatch q, while at large q the FH amplitude is much larger. In Figs. 3(a) and 3(b) we also indicate the soliton existence limit as implied by Eq. (6), i.e., $4k+q>0$ (shown by the crosses on the base plane). It can be seen that the trend of decreasing amplitudes and increasing

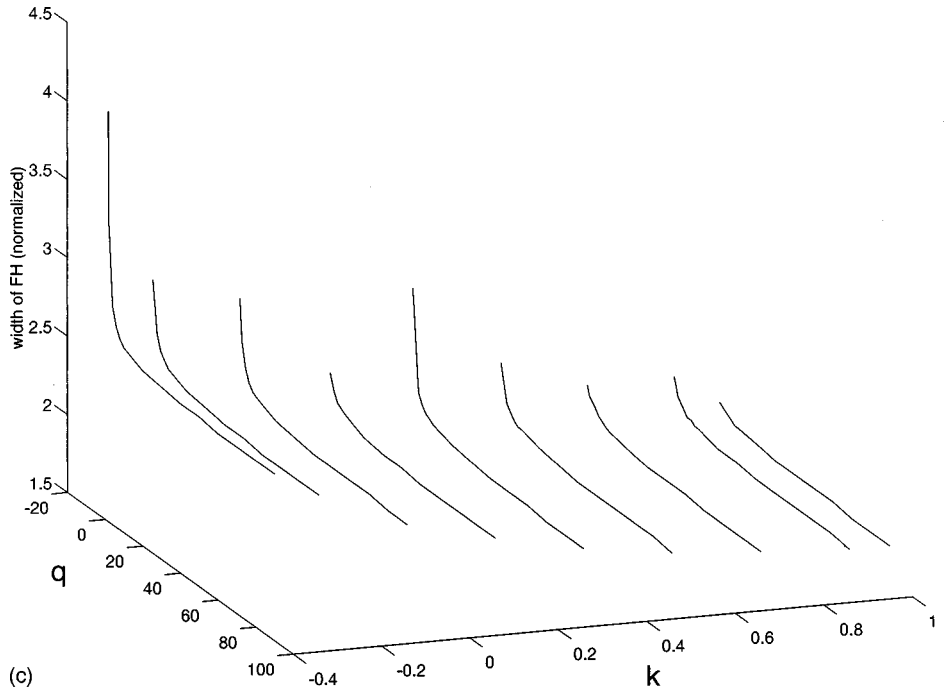

FIG. 3 (*Continued*).

widths accelerates rapidly as this soliton existence limit is approached. A similar trend is observed as another existence limit $k=-1$ is approached, although no curves beyond $k=-0.5$ were drawn because in this region the numerical scheme converges too slowly, which makes it difficult to accumulate enough data for drawing the continuous curves. However, an *opposite* trend is seen as yet another soliton existence limit $k=1$ is approached: The amplitudes and widths keep on increasing and decreasing, respectively, which is quite surprising because from Eq. (6) one would expect that the width should diverge at both limits $k=\pm 1$. This unexpected trend does not reverse up to the value $k=0.99$. At $k=1$, the amplitude remains finite; however, the soliton becomes delocalized with a small finite-amplitude cw oscillatory tail. (Such delocalized soliton solutions were previously discussed in detail in [22].) This in turn is in accord with Eq. (6), which can also be alternatively interpreted as that the exponentially decaying soliton tail is changed to a nonvanishing oscillatory cw. No solutions can be numerically found for $k>1$. However, since a delocalized soliton is not really a soliton and also, as it is shown below, in the same limit the solitons become strongly unstable, the investigation was not carried out further beyond $k>1$. It is relevant to stress that the parametric domain in which the three-wave gap solitons may exist in the present model appears to be completely filled by the soliton solutions. This is a drastic difference from the four-wave model of the $\chi^{(2)}$ gap solitons [7], in which large ''voids'' were found inside the formally available existence domain.

Proceeding to the stability of the fundamental solitons, one sees that it would be really difficult to investigate it analytically (in particular, the VA is much less convenient for this than to search for the shape of stationary solitons). Therefore, the stability was tested by direct simulations of Eqs. (2), using the beam propagation method (BPM). The stationary shape of the solitons produced by the finite-difference numerical solution was used as the initial configuration for the BPM simulations, with an additional perturbation generated by increasing the amplitude of the wave components by 1%. In most cases, the simulations were run over the propagation distance $z=2\pi$ [in the notation of Eqs. (2)], which was quite sufficient to discern between the stable and unstable solitons; however, in some cases, the simulations were run twice as long for stable solitons in order to further check the stability. No change has been observed in the longer simulations as compared to those with $z=2\pi$.

It has been found that when the mismatch q is large enough, the solitons are stable (in agreement with the results reported in [11]). The solitons existing at $k>0$ become unstable as q decreases past a *threshold value* $q_{\rm thr}^{(F)}$ [which depends on the wave-number shift k and slightly on the diffraction coefficient D (see below); the superscript F refers to the fundamental solitons, as another stability threshold for two-solitons will be found below]. For smaller positive values of k, $q_{\rm thr}^{(F)}$ is smaller too and for $k<0$ the threshold does not exist: In this case, *all* the solitons turn out to be stable in the simulations (see more details below). On the other hand, when k gets close to its limit value 1 (see above), $q_{\rm thr}^{(F)}$ becomes very large (i.e., the stability is lost in the limit $k\to 1$ when the soliton demonstrates the unexpected behavior described above). The simulations also demonstrate that the instability of the solitons with q slightly below $q_{\rm thr}^{(F)}$ evolves by developing an asymmetry between the two FH components: For instance, u_1 grows while u_2 diminishes or vice versa. Thus the instability breaks the reduction that leads from Eqs. (3) to Eqs. (4). The asymmetry is enhanced as the waves propagate. For still smaller values of q, the soliton breaks up or develops large distortion very rapidly.

In Fig. 4 we summarize the results found numerically for the stability of the fundamental solitons in the form of their stability and instability domains on the (k,q) (with $k>0$)

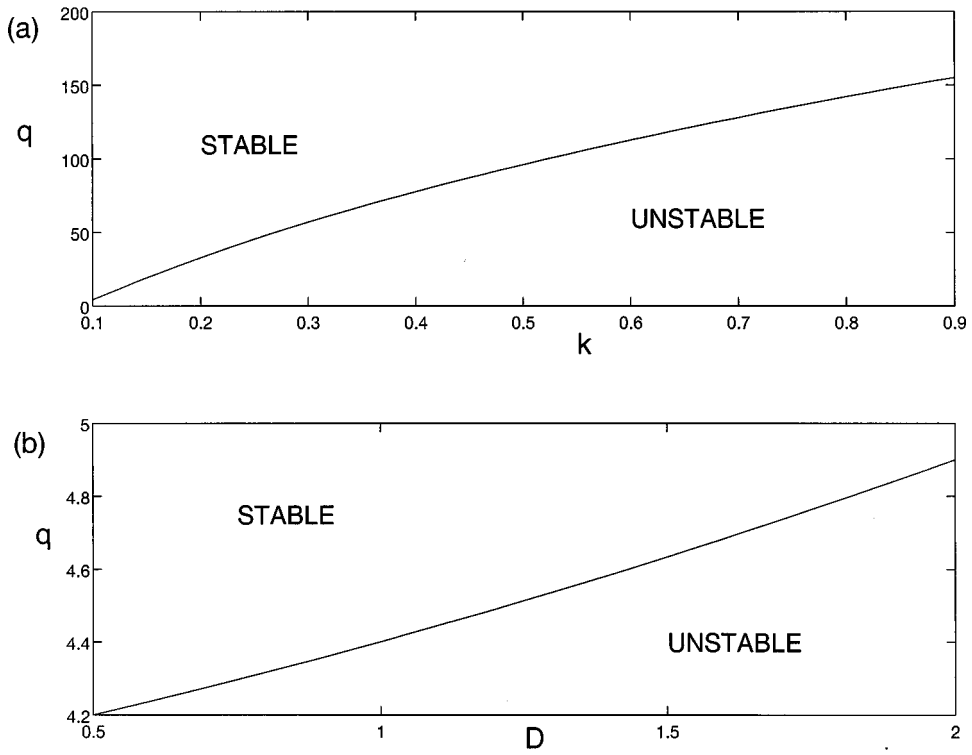

FIG. 4. Numerically found stability domains for the fundamental solitons: (a) on the (q,k) plane at $D=0.5$ and (b) on the (q,D) plane at $k=0.1$.

and (D,q) parametric planes (the presentation of these results in the form of one three-dimensional plot is undesirable because it does not seem clear). Evidently, the borders between the domains simultaneously display the dependences $q_{\rm thr}^{(F)}(k)$ and $q_{\rm thr}^{(F)}(D)$, respectively, With regard to the great difference in the vertical scales between Figs. 4(a) and 4(b), it can be inferred that the diffraction parameter D, unlike the wave-number shift k, has a little effect on $q_{\rm thr}^{(F)}$.

Additional information is given by Fig. 5, where we have redrawn the stability and instability domains (the boundary between them is labeled as the ''stability'' curve consisting of circles) on the (k,q) parametric plane with a different scale, so that the soliton existence limit $4k+q=0$ (shown by crosses and labeled as the ''existence'' curve) and the boundary $q=q_0(k)$ [see Eq. (7)] between the free-tail and tail-locked solitons (the solid line labeled ''tail'') can all be plotted too, $k<0$ being also included. The other two-soliton existence limits $k=\pm 1$ form the left and right boundaries of the figure. In this figure D is fixed at 0.5. Solitons exist above the existence boundary are stable to the left of the stability boundary and are of the tail-locked type above the tail boundary. Note that the free-tail solitons exist only in a narrow stripe. It can be deduced from Eq. (7) that, as D decreases, the curvature of the tail curve reduces (but with the end points at $k=\pm 1$ fixed) and thus the free-tail soliton existence region will further shrink, tending to nothing as $D\to 0$.

The stability and existence curves intersect in Fig. 5 at $(k,q)=(0.08,-0.3)$; thus *all* the solitons at $k<0$ are *stable*, which was verified in many runs of the numerical simulations. It is also noteworthy that, at the negative mismatch $q<0$ there is only a tiny stability domain, at k very close to 0. It is interesting that not all the solitons with the exactly matched harmonics (corresponding to the tail curve) are stable. This situation is drastically different from that known for the usual $\chi^{(2)}$ solitons, which are always stable at the exact-match point [7,8,15]. Also, in the usual $\chi^{(2)}$ models, *all* the tail-locked solitons (corresponding to positive mismatch) and a part of the free-tail ones (that correspond to negative mismatch) are simultaneously stable. This is different from what is depicted here: Only part of both the tail-locked and the free-tail solitons are stable.

VI. TWO-SOLITON STATES

The parametric space of Eqs. (4) was numerically scanned to search for other possible stationary solutions and a family of two-soliton bound states was found. A shape of a typical two-soliton solution is shown in Fig. 6. To describe the whole family of the two-soliton solutions, in Fig. 7 we plot the FH and SH amplitudes, together with the SH width of the individual bound pulses, vs q and D, fixing $k=0.1$. Note that the two individual pulses in the bound state always have equal peak values.

It can be seen that the basic features of the two-soliton solutions are similar to those of the fundamental-soliton ones. The amplitudes of the FH and the SH components increase while the widths decrease, with the increase of q. The effect of changing D is much smaller. As can be expected, the SH amplitude and width decrease and increase, accordingly, with the increase of D, while the FH amplitude and width are only slightly affected by changing D. The soliton existence limit $4k+q=0$ is also included in Figs. 7(a) and 7(b), showing the trend of the solitons to disappear

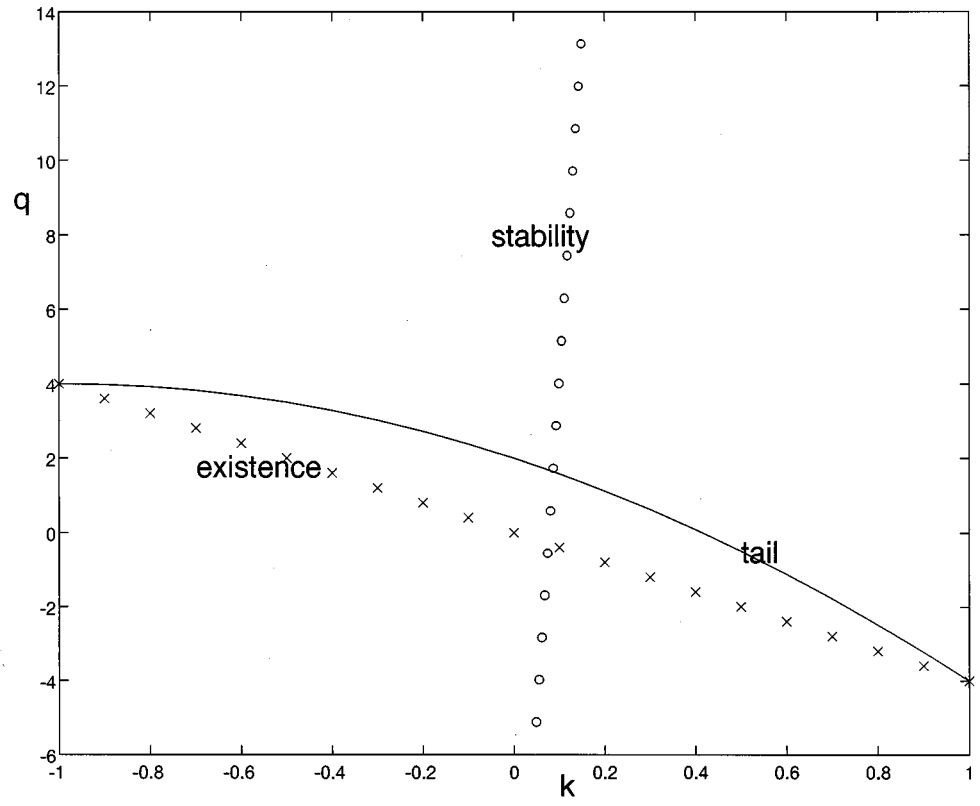

FIG. 5. Numerically determined domains of existence, stability, and tail type for the fundamental solitons on the (q,k) plane at $D=0.5$.

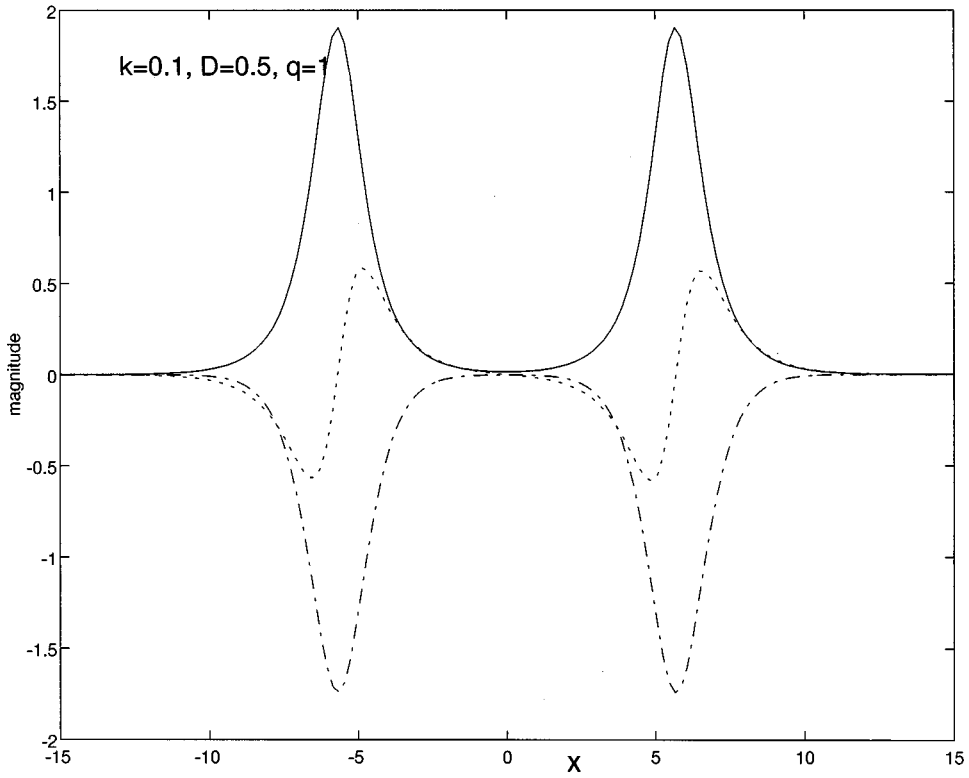

FIG. 6. Typical shape of a numerically found two-soliton at $k=0.1$, $D=0.5$, and $q=1$. The solid and dotted curves are the real and imaginary parts of the FH field u and the dot-dashed curve is the real SH field u_3.

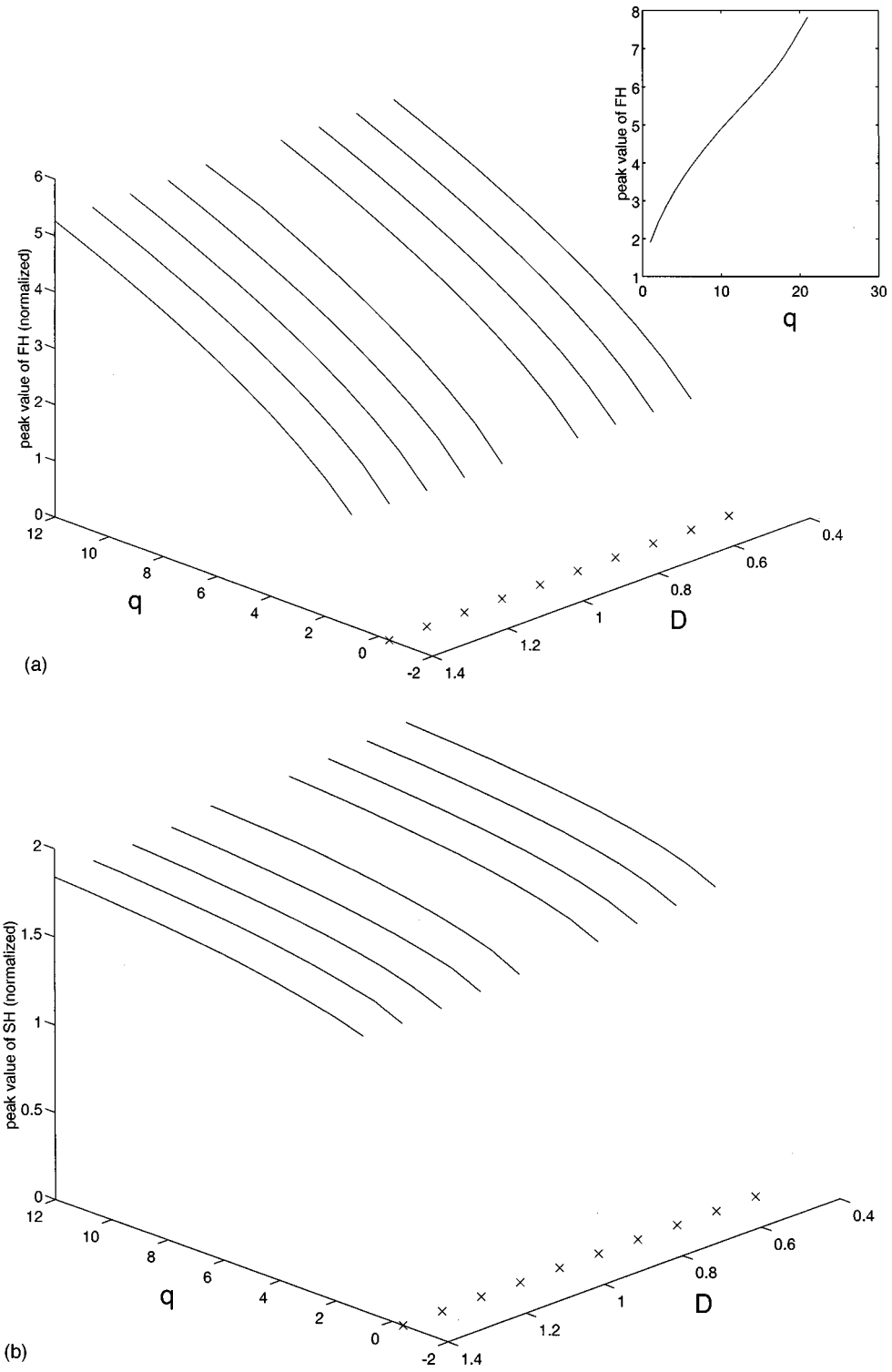

FIG. 7. Family of the two-soliton solutions: (a) the amplitude of the FH (u) field, (b) the amplitude of the SH (u_3) field, and (c) the SH width of the individual bound pulse inside the two-soliton plotted vs the phase mismatch q and the SH diffraction parameter D at a fixed wave-number shift $k=0.1$. The inset in (a) shows an extended plot of the FH amplitude vs q at $D=1$. The line consisting of crosses shows the existence boundary $4k+q=0$ for the free-tail solitons.

by getting infinitely broad and having vanishing amplitudes in this limit. The curves were not traced up to the limit because of the slow convergence of the numerical scheme; however, there is no doubt that this trend persists.

In the limit $q\to\infty$, when the SH field can be eliminated to cast the model into the MTM form [11], the two-solitons *do not* exist because MTM does not have such solutions. This inspires one to search for the two-solitons existence limit for large q and the way they disappear when approaching the limit. In the inset of Fig. 7(a) we show the dependence of the FH amplitudes vs q for $k=0.1$ and $D=1$, with q extended to larger values. It can be seen that the amplitude keeps on increasing and the increase accelerates when at $q\sim 20$. The widths of the waves (not plotted here) are decreasing accord-

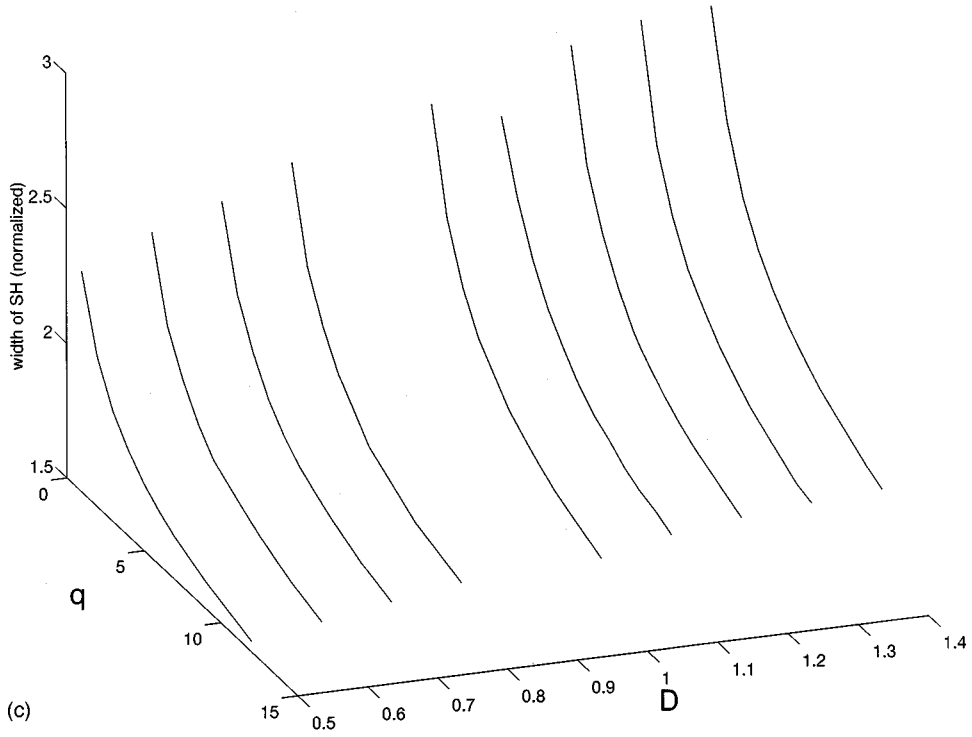

FIG. 7 (*Continued*).

ingly. Thus the trend for the two-solitons is to become taller and narrower as q increases. At $q>20$, the numerical scheme has failed because of an instability caused in it by the large change of the derivatives at the sharp peaks of the pulse. Although an exact existence limit of the two-solitons was not reached at large q, we conjecture that they disappear through a collapselike mechanism, similarly to what is well known in the multidimensional $\chi^{(3)}$ models.

A specific characteristic of the two-soliton is the dependence of the separation S between the individual bound pulses on the model's parameters. The simulations demonstrate that the separation is nearly immune to the changes of the parameters over most of the range considered, except that S slightly decreases with increasing q and increases at those existence limits $k=-1$ and $4k+q=0$ where the fundamental solitons broaden indefinitely. It seems that, near these limits, the individual pulses repel each other more strongly as they spread out. A separate plot of the dependence S vs D is shown in Fig. 8 for $q=10$ and $k=0.1$. It demonstrates an interesting feature that, beyond $D\approx 1.1$, the separation of the pulses rapidly increases with D. This probably indicates a two-solitons existence limit at large D.

The effect of the wave-number shift k on the characteristics of the bound-state solutions was also investigated. Without displaying detailed results, it is sufficient to note the characteristics of the two-solitons vary with k similarly to those of the fundamental solitons (see Fig. 3): With increasing k, the amplitudes increase and the widths decrease. As the existence limits $k=-1$ and $4k+q=0$ are approached, the solitons broaden and amplitudes vanish.

The stability of the two-solitons is a crucially important issue, as similar bound states are also known in the usual (two-wave) $\chi^{(2)}$ model, but they are *always unstable* [16]. On the other hand, a numerically stable object similar to a two-soliton was found in simulations of the four-wave $\chi^{(2)}$ gap-soliton model combining SHG and the Bragg scattering, but completely ignoring the diffraction (dispersion) [7]. We have performed systematic BPM simulations of perturbed two-solitons in order to test their stability in the present model (it is virtually impossible to study the stability analytically, first of all, because the stationary two-soliton is not known in an analytical form). As in the case of the fundamental solitons, the initial perturbation added to the stationary two-solitons was generated by an increase of the amplitudes of the two constituent pulses by 1% and the simulations were then typically run over the propagation distance of $z=2\pi$, which was sufficient to conclude if the two-soliton was stable or not. In many cases when the two-solitons seemed stable, the runs were made twice as long in order to control the accuracy of the results, which, however, never revealed an additional instability.

The stability was first tested for fixed $k=0.1$, while q and D were varied. In addition to the fundamental solitons, the two-solitons are always found to be *stable* at a sufficiently large phase mismatch q, getting destabilized when q decreases past a specific two-soliton threshold value $q_{\rm thr}^{(2)}$. As an illustration, in Figs. 9(a) and 9(b) we show a typical example of the evolution of slightly perturbed stable and unstable two-solitons, corresponding to q taken, respectively, above (at $q=6$) and beneath (at $q=1$) the threshold. Only the FH components are shown in Fig. 9, v_1 being displayed in the region $x<0$ and, simultaneously, v_2 at $x>0$. This way of presenting the numerical results was adopted for convenience; in reality, of course, both components occupy the same space in the medium. It can be seen that the stable two-solitons in Fig. 9(a) maintains its shape and amplitudes, while the two-soliton in Fig. 9(b) clearly develops an insta-

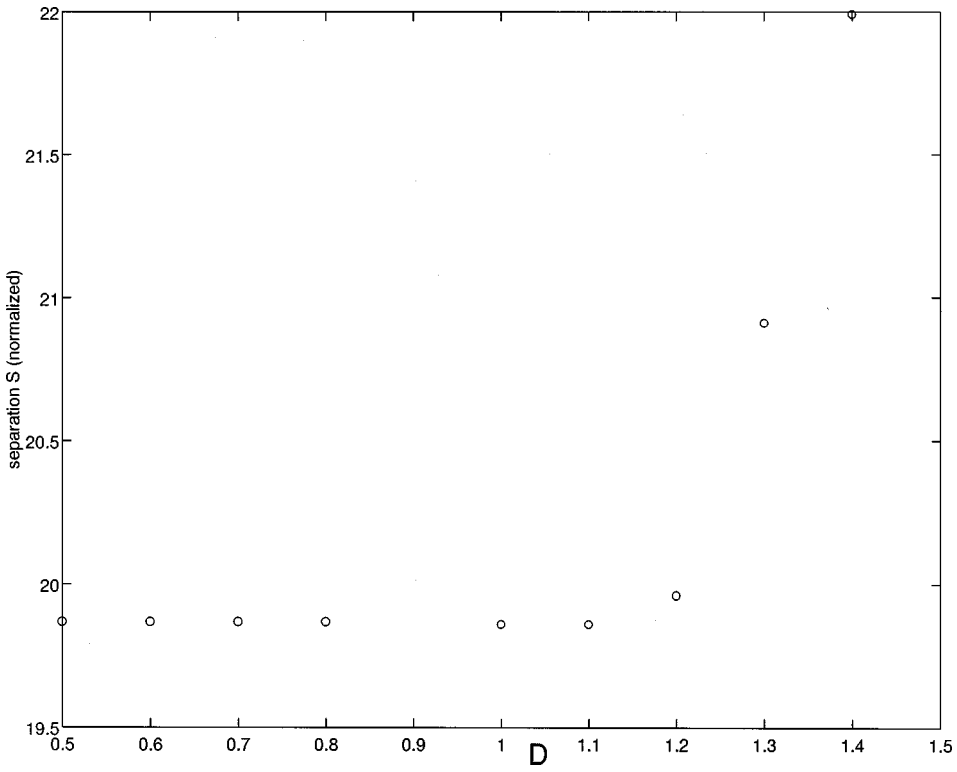

FIG. 8. Separation between the bound pulses inside the two-soliton vs the diffraction parameter D at $k=0.1$ and $q=10$.

bility, developing an asymmetry between v_1 and v_2 (v_2 grows and v_1 diminishes).

The stability threshold $q_{\rm thr}^{(2)}$ is found to be higher than that for the fundamental solitons, although the two thresholds are actually close. The numerically determined stability domain for the two-solitons was plotted on the (q,D) plane in Fig. 10. As D increases, the threshold $q_{\rm thr}^{(2)}$ decreases, although the effect of changing D is actually very weak (note at the vertical scale of Fig. 10). Also, the border between the stable and unstable domains is *obtained* to be practically straight, within our accuracy. It can be seen that $q_{\rm thr}^{(2)}$ decreases towards the threshold value $q_{\rm thr}^{(F)}$ for the fundamental soliton [see Fig. 4(b)], which is quite natural: As it follows from Fig. 8, the two pulses in the two-soliton state separate as D increases, hence the two-soliton stability essentially amounts to the stability of the individual pulses, although the reason why $q_{\rm thr}^{(2)}$ decreases with increasing D, in the range of small D, where the separation between the two individual pulses is quite insensitive to D, is unknown.

For values of k other than 0.1, the stability was also investigated. For $k>0.1$, *all* the two-solitons were found to be unstable, while for $k<0$, they *all* are stable, so that a stability-threshold curve on the (q,k) plane, similar to that drawn in Fig. 4(a) for the fundamental solitons, cannot, as a matter of fact, be obtained for the two-solitons. However, a dependence of the two-solitons stability threshold on the wave-number shift k can be understood by the following argument. For $k=0.1$, it has been found that the threshold $q_{\rm thr}^{(2)}$ is close to but a bit larger than the threshold $q_{\rm thr}^{(F)}$ for the fundamental soliton. For $k=0.3$, the results borrowed from Sec. V yield $q_{\rm thr}^{(F)}=57$. If extrapolation from the $k=0.1$ case is approximately correct, $q_{\rm thr}^{(2)}$ should be >60 for $k=0.3$. Then, of course, no stable two-solitons can be found for $k>0.1$ since the numerical scheme fails to find any stationary two-solution for $q>20$, as mentioned above in the discussion related to the inset in Fig. 7(a). Furthermore, if the two thresholds $q_{\rm thr}^{(2)}$ and $q_{\rm thr}^{(F)}$ are always close, Fig. 5 can be applied, approximately, to the two-solitons too. Recall that Fig. 5 tells us that all the solitons are stable at $k<0$, which exactly complies with the numerical finding that all the two-solitons are also stable if $k<0$.

The last issue to be addressed is the asymmetry between the two FH components, which spontaneously develops as the solitons propagate. Although it cannot be seen in Fig. 9(a), all the stable solitons, *both* fundamental and two-solitons, are found to acquire a nonzero, although small, asymmetry. Because the stability of the two-solitons is a crucially important issue, more simulation runs with an excessively long propagation distance $z=10\pi$ were carried out to see if the asymmetry will keep growing at the parameters values inside the stability domain. A typical example of the evolution of the asymmetry, for $D=0.5, k=0.1$, and $q=10$, is shown in Fig. 11. The asymmetry is quantified by the ratio of the peak values of v_1 and v_2. It can be seen that the ratio approaches a constant value, slightly different from 1, after propagating over a very long distance. A natural assumption that explains this numerical observation is that the underlying equations (3) have a general family of *asymmetric* stationary fundamental-soliton and two-soliton solutions, the solution subject to the above symmetry reduction $u_1=-u_2^*$ being only a particular one. Then a small perturbation breaking the solution's symmetry (generated, e.g., due to an inaccuracy of the numerical scheme) is expected to be neutrally stable, leading to a slightly asymmetric established solution.

Furthermore, a survey of the asymmetry over the whole

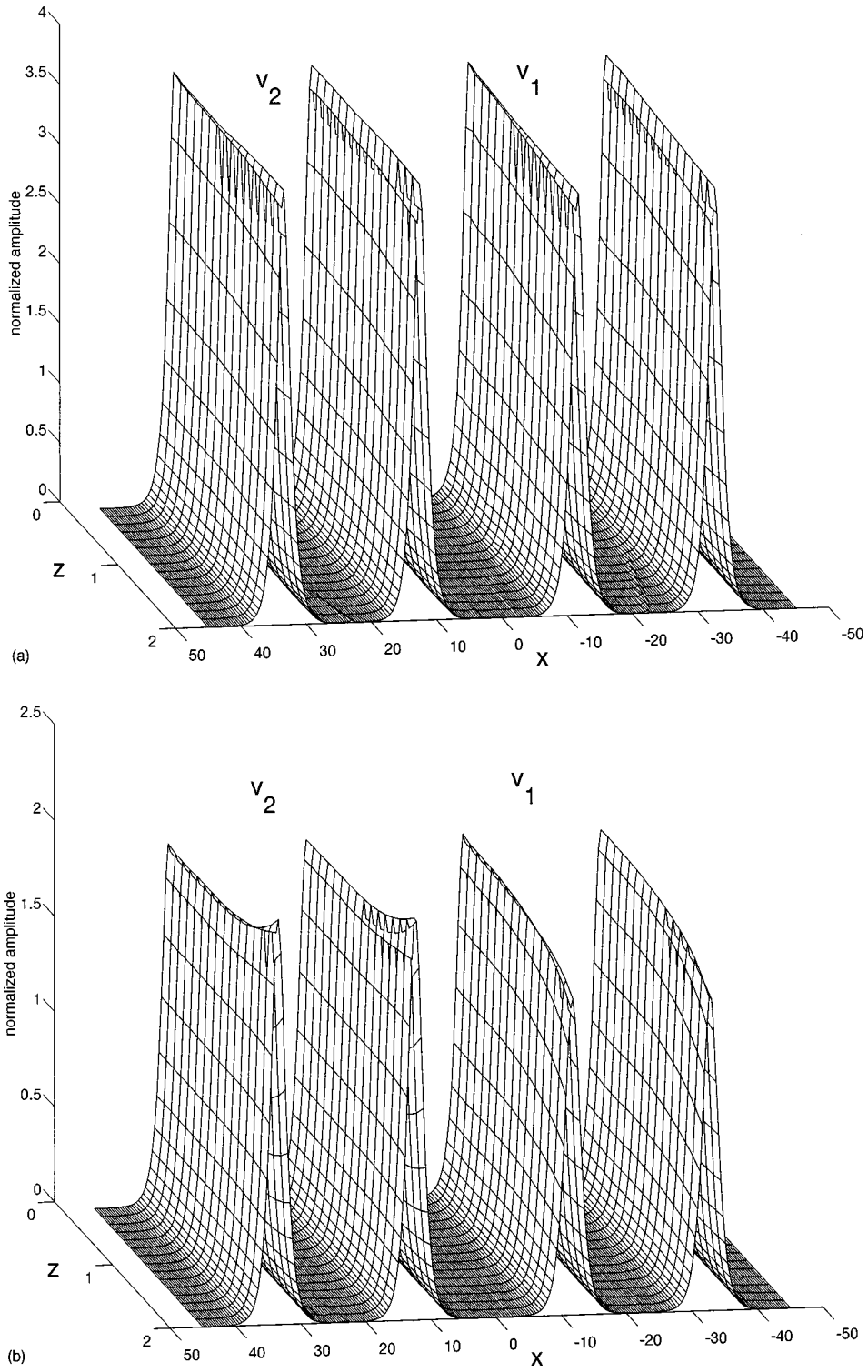

FIG. 9. (a) Evolution of a slightly perturbed two-soliton over a propagation distance of 2π *above* the instability threshold at $k=0.1$, $D=1.2$, and $q=6$. (z is in units of π.) (b) Same as (a), except that $q=1$, i.e., *below* the two-soliton instability threshold.

parameter plane shows that for the stable solitons in the positive k region, the asymmetry is $\sim 1\%$, decreasing as k decreases. In the region of negative k (where the solitons have the trend to be more robust), the observed asymmetry is $\sim 0.1\%$ at $k=-0.1$ and at $k=-0.5$ it drops to $\sim 0.01\%$, which indicates that the soliton have practically no asymmetry. This is another confirmation of the general inference formulated above, according to which the two-solitons are essentially more robust at larger negative k.

VII. CONCLUSION

We have demonstrated the existence of spatial gap solitons, and of their bound states in the form of two-solitons, in a system of three waves, resonantly interacting in a quadratically nonlinear planar waveguide with a Bragg grating written on it. The model includes two components of the fundamental harmonic, with different orientations of their wave vectors, and the second harmonic, whose wave vector is par-

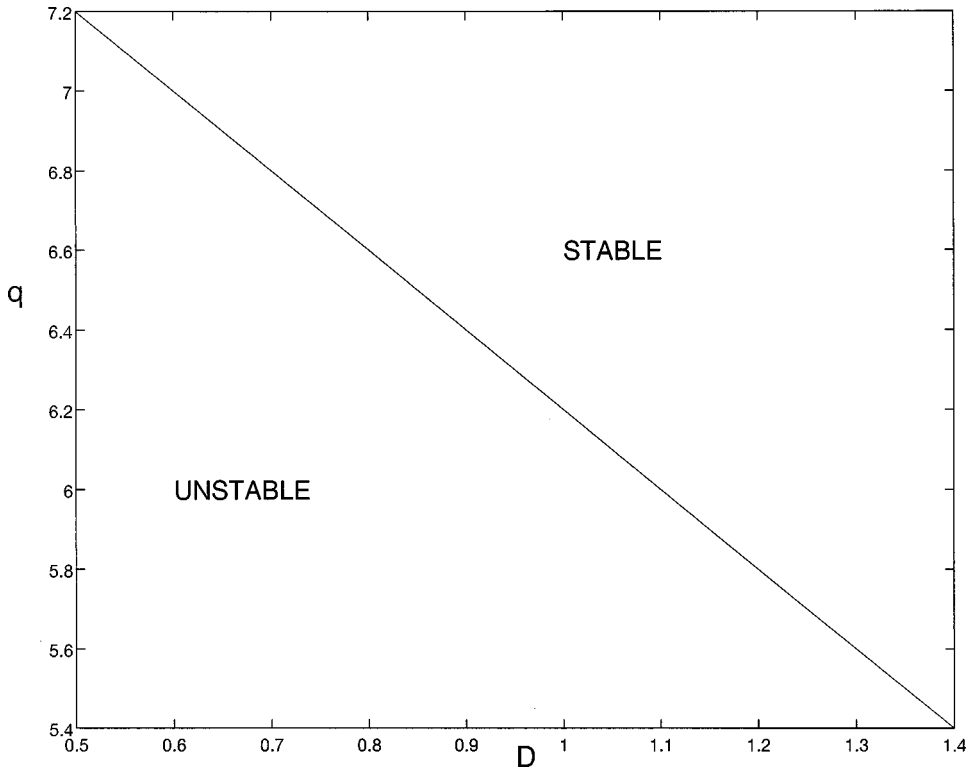

FIG. 10. Numerically determined stability domains for the two-solitons on the (q,D) plane at $k=0.1$.

allel to the grating. Control parameters of the model are the phase mismatch between the harmonics and the diffraction coefficient of the second harmonic that does not interact with the grating. The analysis of the linearized and *semilinearized* versions of the model has allowed us to identify two possible types of solitons, distinguished by the structure of their tails (*free-tail* and *tail-locked* solitons). Then a family of the complex fundamental-soliton solutions was constructed numeri-

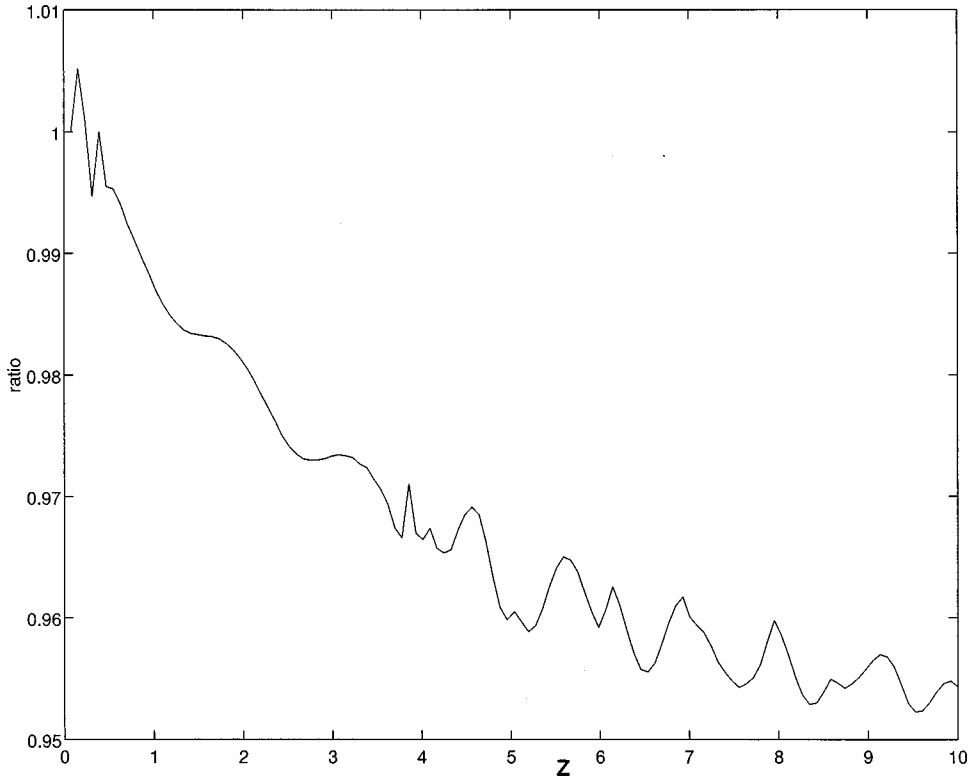

FIG. 11. Evolution of the asymmetry ratio of the two-soliton over a very long propagation distance of 10π well above the instability threshold at $D=0.5$, $k=0.1$, and $q=10$. (z is in units of π.)

cally and analytically by means of the variational approximation, which demonstrates a fairly reasonable agreement with the numerical solutions. This is, as a matter of fact, an example (together with the recent work [23]) of successful application of the variational approximation to the search for *complex* stationary-soliton solutions, in a model where they are not available in an exact form. Soliton existence limits were found in an exact form. Mechanisms by which the fundamental solitons disappear as these limits are approached were explored. Unlike the gap solitons in the four-wave $\chi^{(2)}$ model [7], in the present one the solitons completely fill the domain where they can exist (which implies that they should be easier to observe in the experiment).

Two-soliton solutions also exist in a broad parametric range, with the separation between the bound pulses inside them very weakly depending on the parameters, except for a vicinity of the existence borders. With the increase of the mismatch parameter, the two-solitons display a trend to disappear via a collapse.

The stability of the fundamental solitons and two-solitons was analyzed by means of direct partial differential equation simulations. It was found that both types of solitons are stable or unstable when the mismatch is above or beneath a corresponding threshold value, respectively. The thresholds for the fundamental solitons and two-solitons are different but close, the latter one being somewhat higher. The thresholds strongly depend upon the soliton's wave-number shift k, but are nearly independent of the second-harmonic diffraction coefficient. At $k<0$, the thresholds do not exist as *all* the fundamental solitons and two-solitons are stable. Depending on the parameters, the fundamental soliton at the point of the exact matching between the fundamental and second harmonics (which is, simultaneously, a boundary between the free-tail and tail-locked solitons) may be both stable and unstable, in contrast to the usual $\chi^{(2)}$ models. The existence of *stable* two-soliton bound states is a remarkable feature of the model, which is a drastic difference from the familiar $\chi^{(2)}$ systems. Because a $\chi^{(2)}$ waveguide with the resonant grating can be easily fabricated, the most important physical result of this work is that it suggests straightforward ideas for the experimental search for single- and two-humped three-wave spatial solitons in $\chi^{(2)}$ optical materials by means of the Bragg grating.

The size of the experimental sample necessary for the observation of the solitons is, in any case, no larger than that in which the usual $\chi^{(2)}$ solitons have been observed, i.e., a few centimeters [24], as the effective FH diffraction generated by the grating is stronger than the natural diffraction and hence the corresponding diffraction length, which determines the soliton's size, is smaller than without the grating, while the SH diffraction length is the same as in the usual model. An experimental observation of the solitons in the planar nonlinear waveguides of presently available sizes, with the grating written on them, appears to be quite possible.

ACKNOWLEDGMENT

One of the authors (B.A.M.) appreciates support from the School of Electrical Engineering at the University of New South Wales.

[1] Y. N. Karamzin and A. P. Sukhorukov, Pis'ma Zh. Eksp. Teor. Fiz. **20**, 734 (1974) [JETP Lett. **20**, 339 (1974)]; Zh. Eksp. Teor. Fiz. **68**, 834 (1975) [Sov. Phys. JETP **41**, 414 (1976)].

[2] Y. R. Shen, *The Principles of Nonlinear Optics* (Wiley, New York, 1984), Chap. 6.

[3] S. Trillo and G. Assanto, Opt. Lett. **19**, 1825 (1994); A. L. Belostotsky, A. S. Leonov, and A. V. Meleshko, *ibid.* **19**, 856 (1994); G. Assanto, G. I. Stegeman, M. Sheik-Bahae, and E. Van Stryland, IEEE J. Quantum Electron. **QE-31**, 673 (1995); A. Kobyakov, U. Peschel, and F. Lederer, Opt. Commun. **124**, 184 (1996); A. Kobyakov and F. Lederer, Phys. Rev. A **54**, 3455 (1996); L. Lefort and A. Barthelemy, Electron. Lett. **31**, 910 (1995); G. Assanto, Z. Wang, D. J. Hagan, and E. W. Van Stryland, Appl. Phys. Lett. **67**, 2120 (1995); L. Lefort and A. Barthelemy, Opt. Lett. **20**, 1749 (1995).

[4] D. J. Kaup, Stud. Appl. Math. **55**, 9 (1976).

[5] H. T. Tran, Opt. Commun. **118**, 581 (1995).

[6] B. A. Malomed, D. Anderson, and M. Lisak, Opt. Commun. **126**, 251 (1996).

[7] U. Peschel, C. Etrich, F. Lederer, and B. A. Malomed, Phys. Rev. E **55**, 7704 (1997).

[8] A. V. Buryak, Yu. S. Kivshar, and S. Trillo, Phys. Rev. Lett. **77**, 5210 (1996).

[9] A. V. Buryak and Yu. S. Kivshar, Phys. Rev. Lett. **78**, 3286 (1997).

[10] C. Conti, S. Trillo, and G. Assanto, Phys. Rev. Lett. **78**, 2341 (1997); T. Peschel, U. Peschel, F. Lederer, and B. A. Malomed, Phys. Rev. E **55**, 4730 (1997); H. He and P. D. Drummond, Phys. Rev. Lett. **78**, 4311 (1997); C. Conti, S. Trillo, and G. Assanto, Phys. Rev. E **57**, R1251 (1998).

[11] S. Trillo, Opt. Lett. **21**, 1732 (1996).

[12] W. E. Thirring, Ann. Phys. (N.Y.) **3**, 91 (1958).

[13] A. V. Mikhailov, Zh. Eksp. Teor. Fiz. Pis'ma Red. **23**, 356 (1976); D. J. Kaup and A. C. Newell, Lett. Nuovo Cimento **20**, 325 (1977).

[14] D. N. Christodoulides and R. I. Joseph, Phys. Rev. Lett. **62**, 1746 (1989); A. B. Aceves and S. Wabnitz, Phys. Lett. A **141**, 37 (1989).

[15] D. E. Pelinovsky, A. V. Buryak, and Yu. S. Kivshar, Phys. Rev. Lett. **75**, 591 (1995); L. Torner, D. Mihalache, D. Mazilu, and N. N. Akhmediev, Opt. Lett. **20**, 2183 (1995).

[16] G. I. Stegeman, D. J. Hagan, and L. Torner, Opt. Quantum Electron. **28**, 1691 (1996).

[17] A. V. Buryak and Yu. S. Kivshar, Phys. Lett. A **197**, 407 (1995).

[18] C. R. Menyuk, R. Schiek, and L. Torner, J. Opt. Soc. Am. B **11**, 2434 (1994); C. M. DeSterke and J. E. Sipe, Prog. Opt. **33**, 203 (1994); A. V. Buryak, Ph.D. thesis, Australian National University, 1996 (unpublished).

[19] W. C. K. Mak, B. A. Malomed, and P. L. Chu, Phys. Rev. E **55**, 6134 (1997); **57**, 1092 (1998).

[20] B. A. Malomed and R. S. Tasgal, Phys. Rev. E **49**, 5787 (1994).

[21] W. H. Press, B. P. Flannery, S. A. Teukolsky, and W. T. Vetterling, *Numerical Recipes in C: The Art of Scientific Computing* (Cambridge University Press, Cambridge, 1988).

[22] D. J. Kaup, T. I. Lakoba, and B. A. Malomed, J. Opt. Soc. Am. B **14**, 1199 (1997).

[23] W. C. K. Mak, B. A. Malomed, and P. L. Chu, J. Opt. Soc. Am. B **15**, 1685 (1998).

[24] W. E. Torruellas, Z. Wang, D. J. Hagan, E. W. Van Stryland, G. I. Stegeman, L. Torner, and C. R. Menyuk, Phys. Rev. Lett. **74**, 5036 (1995); R. Schiek, Y. Baek, and G. I. Stegeman, Phys. Rev. E **53**, 1138 (1996).